

A study of the relaxation dynamics in a quadrupolar NMR system using Quantum State Tomography

R. Auccaise^a, J. Teles^b, R.S. Sarthour^a, T.J. Bonagamba^b, I.S. Oliveira^a, E.R. deAzevedo^{b,*}

^a Centro Brasileiro de Pesquisas Físicas, Rua Dr. Xavier Sigaud 150, Rio de Janeiro 22290-180, RJ, Brazil
^b Instituto de Física de São Carlos, Universidade de São Paulo, P.O. Box 369, São Carlos 13560-970, SP, Brazil

Received 29 October 2007; revised 11 January 2008
Available online 30 January 2008

Abstract

This article reports a relaxation study in an oriented system containing spin 3/2 nuclei using quantum state tomography (QST). The use of QST allowed evaluating the time evolution of all density matrix elements starting from several initial states. Using an appropriated treatment based on the Redfield theory, the relaxation rate of each density matrix element was measured and the reduced spectral densities that describe the system relaxation were determined. All the experimental data could be well described assuming pure quadrupolar relaxation and reduced spectral densities corresponding to a superposition of slow and fast motions. The data were also analyzed in the context of Quantum Information Processing, where the coherence loss of each qubit of the system was determined using the partial trace operation.

© 2008 Elsevier Inc. All rights reserved.

Keywords: NMR Quantum Information Processing; Quantum State Tomography; Relaxation dynamics; Quadrupolar spin 3/2 oriented system

1. Introduction

Nuclear Magnetic Resonance (NMR) has been successfully used as an experimental method for many Quantum Information Processing (QIP) implementations [1,2]. This includes the implementation of many quantum algorithms [3–8], execution of quantum simulations [9–11], and also testing of quantum protocols [12]. While n coupled spin 1/2 nuclei, either in solid or liquid state, have been extensively used to process the information of an n qubit system, single quadrupolar nuclei with spin $I > 1/2$ have been used to process the information of a $\log_2(2I + 1)$ equivalent qubit system. In both cases, an important aspect concerning QIP applications is the maintenance of the quantum state coherence for long times compared with the duration of the desired quantum operations. In this sense, the loss of coherence and the energy dissipation by the spin quantum

system (i.e., relaxation) play a major role. Recently, theoretical as well as experimental studies about the nature of the spin-environment coupling have been reported [13–21]. Of course, NMR relaxation is a well known phenomenon and its basis was established in early reports [22–26]. Regarding quadrupolar relaxation, one can point out the pioneer study published by Pople et al. [26], that explained the strong line broadening observed in $I > 1/2$ spin systems using quadrupolar relaxation. Following this idea, many other theoretical treatments about the relaxation phenomena in quadrupolar systems were presented [27–29]. More sophisticated relaxation studies in quadrupolar systems were performed for anisotropic media using two-dimensional quadrupolar spectroscopy [30] and multiple quantum spectroscopy [31]. Recent reviews about relaxation processes have also been published for $I = 3/2$ systems [32,33]. In these studies, the characterization of the relaxation process is performed by means of reduced spectral densities, which contain the information about the local field fluctuations [34], and, thus, are the main parameters to be determined. Despite the NMR relaxation

* Corresponding author.

E-mail addresses: auccais@cbpf.br (R. Auccaise), azevedo@ifsc.usp.br (E.R. deAzevedo).

theory as well as its implications are well known, there are only few studies in the context of Quantum Computing and Quantum Information [13–17,35–37]. Thus, a straight question that could be drawn is how the NMR relaxation parameters correlate with the decoherence times of the individual NMR qubits. Another point concerns the ability that a quadrupolar system has to emulate the relaxation of other quantum systems. In both cases, density matrix tomography, also known as Quantum State Tomography (QST), is very useful because it makes possible to determine independently all density matrix elements, so that their relaxations can be monitored individually. In this article we present a relaxation study of a spin 3/2 quadrupolar system in the context of QIP. For that, several pseudo-pure states were prepared using numerically optimized pulses known as Strongly Modulated Pulses (SMP) [38,39]. More specifically, we experimentally followed the time evolution of the pseudo-pure states corresponding to $|00\rangle$, $|01\rangle$, $|10\rangle$, $|11\rangle$, $\frac{1}{2}(|00\rangle + |01\rangle + |10\rangle + |11\rangle)$, and $\frac{1}{\sqrt{2}}(|00\rangle + |11\rangle)$. Then, by fitting the experimental data using a set of equations based on the Redfield theory [25], the reduced spectral densities were determined. The obtained spectral densities are consistent with a previously reported relaxation model for nematic liquid crystals [54,56] that accounts for the presence of a slow and fast motion components. In the last part of the article, the questions concerning the qubit relaxation in a spin 3/2 quadrupolar system emulating the relaxation of a spin 1/2 is addressed.

2. Theory

The Hamiltonian that describes a $I > 1/2$ spin system in the laboratory frame, considering Zeeman and first order quadrupolar interaction can be expressed as [40]:

$$\mathcal{H} = -\hbar\omega_L I_z + \frac{\hbar\omega_Q}{6} (3I_z^2 - I(I+1)). \quad (1)$$

The first term describes the Zeeman interaction and the second the static first order quadrupolar interaction (with quadrupolar frequency of ω_Q). Hence, for nuclear spin $I = 3/2$ the eigenvectors of the Zeeman plus quadrupolar terms are $|3/2\rangle$, $|1/2\rangle$, $|-1/2\rangle$, and $|-3/2\rangle$, which can be labeled as $|00\rangle$, $|01\rangle$, $|10\rangle$, and $|11\rangle$, corresponding to a two-qubit system (see Fig. 1). For describing the relaxation

one needs to consider a random coupling of this system with a relaxation reservoir. For example, assuming pure quadrupolar relaxation, the Hamiltonian that describes this coupling can be explicitly written in a general form as [40]:

$$\mathcal{H}_1(t) = \sum_{m=-2}^{m=+2} F^{(m)}[\alpha(t), \beta(t), \gamma(t)] A^{(m)}, \quad (2)$$

$$A^{(0)} = [3I_z^2 - I(I+1)], \quad (3)$$

$$A^{(\pm 1)} = \frac{\sqrt{6}}{2} [I_z I_{\pm} + I_{\pm} I_z], \quad (4)$$

$$A^{(\pm 2)} = \frac{\sqrt{6}}{2} I_{\pm}^2, \quad (5)$$

where the lattice functions $F^{(m)}$ depend on the elements of the electric field gradient tensor. $\alpha(t)$, $\beta(t)$, and $\gamma(t)$ stand for the Euler angles relating the molecule/nucleus orientation with respects to the laboratory frame [40]. The system dynamics under the presence of relaxation processes can be described using the Redfield formalism [25,40] for the reduced density matrix $\rho_{\alpha\alpha'}$. Here the term reduced density matrix refers to the density matrix without considering the term proportional to the identity in its operator expansion:

$$\rho_{\alpha\alpha'}^{\text{full}} = \frac{1}{Z} \mathbf{1} + \frac{1}{k_B T} \rho_{\alpha\alpha'}, \quad (6)$$

where Z is the partition function. Just for the sake of simplicity from now on we will refer to the reduced density matrix simply as density matrix $\rho_{\alpha\alpha'}$. According to the Redfield theory, the time evolution of each element of $\rho_{\alpha\alpha'}$ is given by the solution of the following differential equation:

$$\frac{\partial \rho_{\alpha\alpha'}(t)}{\partial t} = \sum_{\beta\beta'} R_{\alpha\alpha'}^{\beta\beta'} e^{i(\omega_{\alpha} - \omega_{\beta} + \omega_{\beta'} - \omega_{\alpha'})t} \rho_{\beta\beta'}(t), \quad (7)$$

where $R_{\alpha\alpha'}^{\beta\beta'}$ represents the element $\alpha\alpha'\beta\beta'$ of the relaxation superoperator with $\alpha, \alpha', \beta, \beta' = 0, 1, 2, 3$ and ω_{α} , $\omega_{\alpha'}$, ω_{β} , $\omega_{\beta'}$ correspond to eigenvalues of the Zeeman plus quadrupolar Hamiltonians [40,25]. The explicit relaxation superoperator depends on the specific interactions that drive the relaxation process and also on the correlation times of the local field fluctuations. This can be taken into account by writing the corresponding relaxation matrix in terms of a set of reduced spectral densities and coupling strengths, whose the explicit expressions depend on the interaction motion model that drives the relaxation, i.e., the relaxation mechanism. Although the main relaxation mechanism for spins $I > 1/2$ is usually the quadrupolar interaction, in many cases dipolar relaxation cannot be neglected. However, in systems where the quadrupolar interaction is much stronger than the dipolar couplings, the former can be assumed as the single relaxation mechanism. This is the case of the present article, where the quadrupolar frequency $\nu_Q = \frac{\omega_Q}{2\pi}$ (≈ 17 kHz, estimated from the satellite lines) is much higher than the dipolar fields (< 100 Hz, estimated from the line width of the central transition) (see

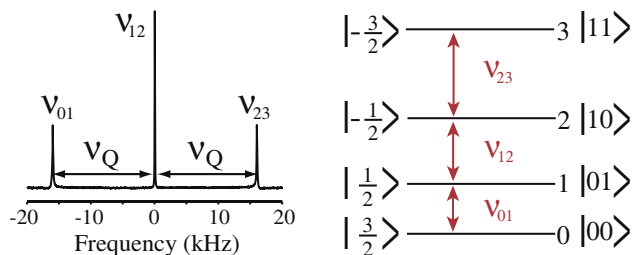


Fig. 1. ^{23}Na NMR spectrum of the oriented liquid crystal sample (Sodium Dodecyl Sulfate, SDS) and the corresponding energy diagram with the quantum state labeling.

Fig. 1). There are many reports considering pure quadrupolar relaxation, i.e., assuming that the loss of coherence and energy dissipation by the spin system are exclusively due to electric field gradient fluctuations [41,27,40,42]. In the case of pure quadrupolar relaxation in spin 3/2 systems, $|\omega_Q| \ll |\omega_L|$, the relaxation can be described by three reduced spectral densities at the Larmor frequency: J_0 , J_1 , and J_2 [43]. These reduced spectral densities depend on specific models for the molecular motions that induced the field fluctuations. Meanwhile we will just assume pure quadrupolar relaxation, leaving the discussion on the evaluation of the reduced spectral densities and specific relaxation model for the next sections. In [41] the relaxation matrices for all quantum coherences were derived considering that the quadrupolar interaction, represented by the Hamiltonian shown in Eq. (2), was the only relaxation mechanism. A further development was presented in reference [43] that shows a derivation of the expressions that describe the relaxation dynamics of the density elements obtained by diagonalization of the relaxation matrices. It was shown for pure quadrupolar relaxation that the solution of the Redfield Eq. (7) with the three above reduced spectral densities can be summarized as:

$$\rho_{01}(t) = \frac{1}{2}[\rho_{01}(t_0) + \rho_{23}(t_0) + (\rho_{01}(t_0) - \rho_{23}(t_0))e^{-2CJ_2(t-t_0)}]e^{-C(J_0+J_1)(t-t_0)}, \quad (8)$$

$$\rho_{23}(t) = \frac{1}{2}[\rho_{01}(t_0) + \rho_{23}(t_0) - (\rho_{01}(t_0) - \rho_{23}(t_0))e^{-2CJ_2(t-t_0)}]e^{-C(J_0+J_1)(t-t_0)}, \quad (9)$$

$$\rho_{02}(t) = \frac{1}{2}[\rho_{02}(t_0) + \rho_{13}(t_0) + (\rho_{02}(t_0) - \rho_{13}(t_0))e^{-2CJ_1(t-t_0)}]e^{-C(J_0+J_2)(t-t_0)}, \quad (10)$$

$$\rho_{13}(t) = \frac{1}{2}[\rho_{02}(t_0) + \rho_{13}(t_0) - (\rho_{02}(t_0) - \rho_{13}(t_0))e^{-2CJ_1(t-t_0)}]e^{-C(J_0+J_2)(t-t_0)}, \quad (11)$$

$$\rho_{12}(t) = \rho_{12}(t_0)e^{-C(J_1+J_2)(t-t_0)}, \quad (12)$$

$$\rho_{03}(t) = \rho_{03}(t_0)e^{-C(J_1+J_2)(t-t_0)}, \quad (13)$$

$$\rho_{00}(t) = 3p - \frac{1}{4}[R_1^0 e^{-2C(J_1+J_2)(t-t_0)} - R_2^0 e^{-2CJ_2(t-t_0)} - R_3^0 e^{-2CJ_1(t-t_0)}], \quad (14)$$

$$\rho_{11}(t) = p + \frac{1}{4}[R_1^0 e^{-2C(J_1+J_2)(t-t_0)} + R_2^0 e^{-2CJ_2(t-t_0)} - R_3^0 e^{-2CJ_1(t-t_0)}], \quad (15)$$

$$\rho_{22}(t) = -p + \frac{1}{4}[R_1^0 e^{-2C(J_1+J_2)(t-t_0)} - R_2^0 e^{-2CJ_2(t-t_0)} + R_3^0 e^{-2CJ_1(t-t_0)}], \quad (16)$$

$$\rho_{33}(t) = -3p - \frac{1}{4}[R_1^0 e^{-2C(J_1+J_2)(t-t_0)} + R_2^0 e^{-2CJ_2(t-t_0)} + R_3^0 e^{-2CJ_1(t-t_0)}], \quad (17)$$

where $p = \langle i|\rho^{\text{eq}}|i\rangle/(2m)$, with m being the corresponding I_z eigenvalues and the superscript eq denotes the thermal equilibrium state. ρ_{ij} 's are the density matrix

elements with the index values $i, j = 0, 1, 2, 3$ corresponding to the states $|3/2\rangle$, $|1/2\rangle$, $|-1/2\rangle$, and $|-3/2\rangle$, respectively. The parameter C is a proportionality coefficient that depends on the quadrupolar coupling constant as [43]:

$$C = \frac{\chi_Q^2}{40} \left(1 + \frac{\eta_Q^2}{3}\right), \quad \chi_Q = \frac{e^2 q Q}{\hbar} \quad (18)$$

Again, χ_Q is the quadrupole coupling constant and η_Q is the asymmetry parameter of the quadrupolar interaction.

2.1. Determination of the reduced spectral densities from the relaxation data

QST allows experimentally following the evolution of all the density matrix elements. Thus, by fitting the experimental data with Eqs. (8)–(17) it is possible to determine the reduced spectral densities. However, the inconvenience of directly using such equations is that most of them show multi-exponential decay, which can lead to ambiguous fittings. Fortunately, Eqs. (8)–(17) can be combined to provide single-exponential functions, i.e.,

$$\rho_{01}(t) + \rho_{23}(t) = A_1 e^{a_1 t}, \quad (19)$$

$$\rho_{02}(t) + \rho_{13}(t) = A_2 e^{a_2 t}, \quad (20)$$

$$\rho_{12}(t) = A_3 e^{a_3 t}, \quad (21)$$

$$\rho_{03}(t) = A_4 e^{a_3 t}, \quad (22)$$

which can be linearized to give the following J_n dependent coefficients,

$$a_1 = -C(J_0 + J_1), \quad (23)$$

$$a_2 = -C(J_0 + J_2), \quad (24)$$

$$a_3 = -C(J_1 + J_2). \quad (25)$$

The amplitudes are given by $A_1 = \rho_{01}^0 + \rho_{23}^0$, $A_2 = \rho_{02}^0 + \rho_{13}^0$, $A_3 = \rho_{12}^0$, and $A_4 = \rho_{03}^0$.

An analogous treatment can be used for the diagonal elements, which gives:

$$\rho_{00}(t) + \rho_{11}(t) - \rho_{22}(t) - \rho_{33}(t) = 2p + R_2^0 e^{-2CJ_2 t}, \quad (26)$$

$$-\rho_{00}(t) + \rho_{11}(t) + \rho_{22}(t) - \rho_{33}(t) = R_1^0 e^{-2C(J_1+J_2)t}, \quad (27)$$

$$\rho_{00}(t) - \rho_{11}(t) + \rho_{22}(t) - \rho_{33}(t) = p + R_3^0 e^{-2CJ_1 t}. \quad (28)$$

Therefore, if the quadrupolar parameters χ_Q and η_Q are known, the reduced spectral densities J_0 , J_1 , and J_2 can be independently found from Eqs. (19)–(22). Furthermore, the J_1 and J_2 values can be compared with that ones obtained from (26)–(28) to check the consistency of the experimental data with the adopted relaxation model.

3. Experiments

3.1. Experimental procedures

The ^{23}Na NMR experiments were performed using a magnetic field oriented lyotropic liquid crystal system

(Sodium Dodecyl Sulfate, SDS), using a 9.4 T—VARIAN INOVA spectrometer. The sample composition was 21.3% of SDS, 3.6% of decanol, and 75.1% of deuterium oxide [54]. The quadrupolar coupling was found to be (16700 ± 70) Hz at 24 °C. In the experiments that characterized the relaxation of all elements of the density matrix, a initial pseudo-pure state corresponding to superposition state $|\text{sup}\rangle \equiv \frac{1}{2}(|00\rangle + |01\rangle + |10\rangle + |11\rangle)$ was prepared using the SMP technique [38,39,44]. In this case, all the density matrix elements were measured using the QST method via coherence selection [44]. In the experiments that characterized only the relaxation of the diagonal density matrix elements, initial states that have populations corresponding to the states $|00\rangle$, $|01\rangle$, $|10\rangle$, $|11\rangle$, and the cat state $|\text{cat}\rangle \equiv \frac{1}{\sqrt{2}}(|00\rangle + |11\rangle)$ were prepared. In this case, the SMP optimizations and the tomography [44] were performed just for the populations. The initial states populations and the full tomographed density matrix for the state $|\text{sup}\rangle$ are shown in Fig. 2.

The basic experimental scheme shown in Fig. 3 consisted of: a state preparation period performed with SMP; a variable evolution period τ where relaxation takes place; a hard RF pulse with the correct phase cycling and duration to execute QST via coherence selection [44]. For off-diagonal elements, a π pulse was added in the middle of the evolution period to refocus the B_0 field inhomogeneities. Because quadrupolar evolution is not refocused by the π

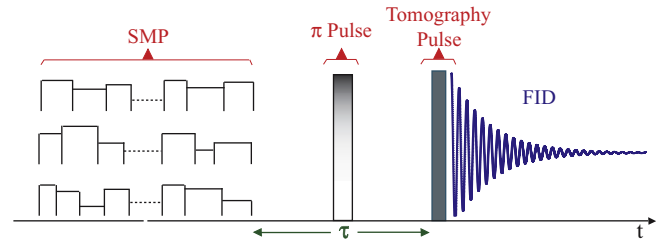


Fig. 3. Scheme of the pulse sequence used for probing the relaxation of the individual density matrix elements. The initial states are prepared with the SMP technique [38]. The state relaxation takes place during a variable evolution period and, finally, a hard RF pulse with the correct phase cycling and duration is applied to execute QST via coherence selection [44].

pulse, evolution periods multiple of $2\pi/\omega_Q$ were used. For diagonal elements, no π pulse was applied.

3.2. Experimental results

3.2.1. Quadrupolar parameters in lyotropic liquid crystals

As described in the previous section, in order to obtain the reduced spectral densities via QST it is necessary to know the constant C , which is defined in terms of the quadrupolar coupling constant χ_Q and the asymmetry parameter η_Q [53]. For nematic liquid crystals such as used in this article (SDS), these parameters can be obtained from the quadrupolar splitting $\nu_Q = \frac{\omega_Q}{2\pi}$ if the exact nematic phase and the orientational order parameter are known [54]. For the sample composition used here, the liquid crystal may be in two uniaxial nematic phases (see the phase diagram in reference [54] and the sample composition in the experimental section), named calamitic (N_C) and discotic (N_D). Since both phases are uniaxially orientated one can assume $\eta_Q \approx 0$, as confirmed by observing the NMR spectra as a function of the orientation in references [55,54]. Note that since η_Q is only used to calculate the C constant, if $\eta_Q \neq 0$ the C value can be underestimated at most by a factor of 1/3. For $\eta_Q < 0.5$, which is mostly like the case of our system, the underestimation factor is smaller than 0.08, which will have little effect in the determination of the spectral densities. The nematic phase can be identified by observing the evolution of the ^{23}Na NMR spectra [54] as the macroscopic orientation of the sample increases due to the presence of the NMR magnetic field. Immediately after the sample is placed in the magnetic field, the ^{23}Na spectra has a characteristic powder line shapes, but show a progressive evolution from that to the three line spectra expected for an oriented liquid crystal (Fig. 1). In the present case the total time of this transition was typically 1 h. For uniaxially oriented liquid crystals the quadrupolar splitting ν_Q is given by [54]:

$$\nu_Q = \frac{1}{8\pi} (3\cos^2\theta_{LD} - 1) S_{DN} \bar{\chi}_Q, \quad (29)$$

where θ_{LD} is the angle between the local nematic director with the magnetic field, $\bar{\chi}_Q$ is the residual quadrupolar coupling constant (in rad/s) and S_{DN} is an order parameter that depends on the shape and order of the micelles in

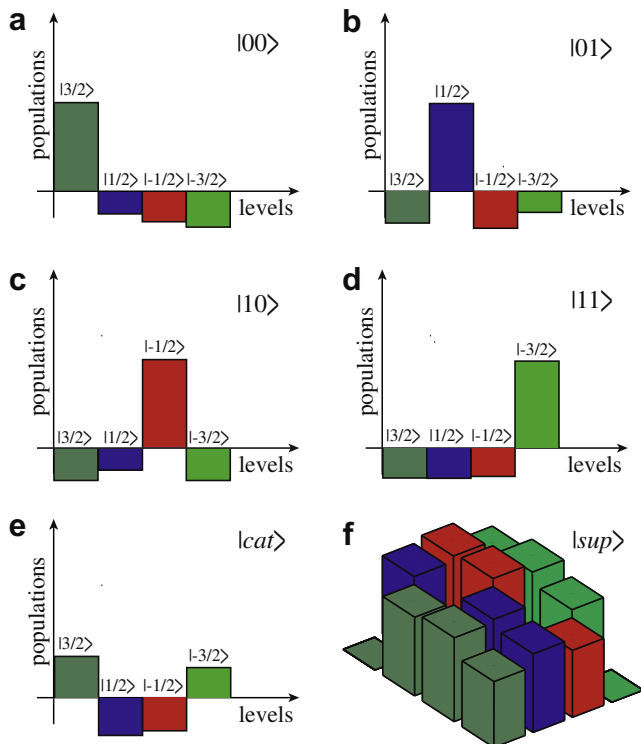


Fig. 2. Experimental diagonal elements of the density matrices (populations) corresponding to the quantum states (a) $|00\rangle$; (b) $|01\rangle$; (c) $|10\rangle$; (d) $|11\rangle$; and (e) $|\text{cat}\rangle$. (f) Experimental real part of the density matrix corresponding to the state $|\text{sup}\rangle$. Note that the density matrix shown are only the part detected by NMR, i.e., the second term in the right side of Eq. (6).

the nematic liquid crystal [54]. In the N_C phase the director is aligned with the magnetic field ($\theta_{LD} = 0$). Thus, for a N_C phase, the quadrupolar splitting in the oriented sample increases twice from its initial value measured in the powder pattern. In contrast, since for the N_D phase $\theta_{LD} = 90^\circ$, ν_Q does not change as the sample orients in the magnetic field [54]. In our case the expected increase in ν_Q was observed, so one can assign the sample as being in the N_C phase. However, the determination of $\bar{\chi}_Q$ also requires the knowledge of S_{DN} . The simultaneous determination of $\bar{\chi}_Q$ and S_{DN} can be done by measuring ν_Q for different orientations of the director relative to the magnetic field. This has been already done in reference [54] where it was found that $S_{DN} = -0.30 \pm 0.02$ for the N_C phase at 24 °C. Since in our ^{23}Na NMR spectrum at 24 °C $\nu_Q = (16700 \pm 70)$ Hz, we found $\chi_Q = (-7.0 \pm 0.5) \times 10^5$ rad/s. Hence, using Eq. (18) one find $C = (1.2 \pm 0.1) \times 10^{10} \text{s}^{-2}$.

3.2.2. Evaluation of the reduced spectral densities

In order to monitor the coherence loss of the off-diagonal density matrix elements, we experimentally determined the time evolution of each element starting from the uniform superposition of states, $|\text{sup}\rangle$ (see Fig. 2). The experimental data were combined according to (19)–(22) and fitted by exponential functions to determine the coefficients a_1 , a_2 , and a_3 . The combined experimental curves and the corresponding fittings are shown in Fig. 4. The reduced spectral densities J_n obtained by the adjust of Eqs. (19)–(22) and using $C = (1.2 \pm 0.1) \times 10^{10} \text{s}^{-2}$ are shown in the *coherences* column of Table 1. The same procedure was used to find J_1 and J_2 via the *populations* data using

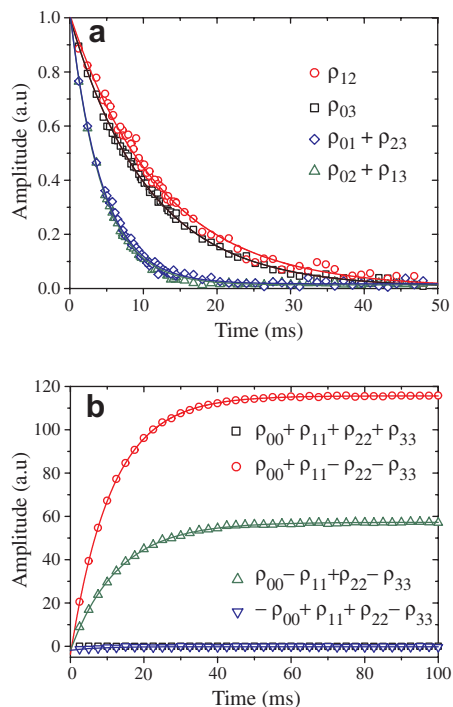


Fig. 4. Combined density matrix elements starting from the $|\text{sup}\rangle$ state. Experimental data (symbols) and corresponding fittings (solid lines). The fittings were performed using Eqs. (19)–(22) and (26)–(28).

Table 1

Reduced spectral densities obtained from the relaxation of the density matrix diagonal elements (*populations* column) and from the off-diagonal elements (*coherences* column) of the superposition states

	<i>Coherences</i>	<i>Populations</i>	<i>Average</i>
$J_0(10^{-9} \text{s})$	14 ± 1	—	14 ± 1
$J_1(10^{-9} \text{s})$	4 ± 1	3.8 ± 0.4	3.9 ± 0.7
$J_2(10^{-9} \text{s})$	3.4 ± 0.5	3.6 ± 0.3	3.5 ± 0.4

Eqs. (26)–(28), which gave the values in the *populations* column of Table 1. The lower errors in the *populations* column is due to the fact that only Eqs. 26 and 28 were used to evaluate the reduced spectral densities in this case. For the superposition state, the Eq. (27) is almost constant along the relaxation period, making it inappropriate to give reasonable values for the reduced spectral densities.

Using the averaged reduced spectral densities and the previous knowledge of the initial density matrix, one can test the validity of the pure quadrupolar relaxation model for describing the system decoherence by replacing these values in Eqs. (8)–(17) and comparing with the experimental curves of Fig. 5.

The same procedure was performed for the populations of all the other states shown in Fig. 2. However, since in these cases only the diagonal elements need to be probed, only the populations were optimized by the SMP technique and tomographed (see Fig. 2). The reason for that was to produce states with higher population differences in order to minimize the fitting errors and enhance the multi-exponential behavior of the populations relaxation. The extracted reduced spectral densities are shown in Table 2.

Similarly as before, we used the reduced spectral densities, the initial density matrix, and Eqs. (14)–(17) to reproduce the experimental relaxation of the diagonal elements. This is shown in Fig. 6 for populations corresponding to the states $|00\rangle$, $|01\rangle$, $|10\rangle$, $|11\rangle$, and $|\text{cat}\rangle$. In all cases the experimental behavior was well reproduced using Eqs. (14)–(17).

By inspection of Eqs. (8)–(13), we can see that for all the density matrix coherences the single-exponential decay is always expected for an initial state like $|\text{sup}\rangle$. This is due to the equal amplitudes that enter in Eqs. (8)–(13) and cancel the exponential factor inside the brackets. However, as in the present case $J_0 > J_1 \approx J_2$, even for an arbitrary initial state, a multi-exponential decay should be more easily recognized for the populations than for the coherences, see Fig. 6. In fact, this is a most fundamental behavior that can be explained, via the Redfield theory, without assuming any specific model for the relaxation mechanisms. In that formalism, by using the secular approximation, i.e., assuming that the internal interactions are much greater than the relaxation rates, one can show that all cross-terms in Eq. (7) can be neglected for the coherence elements, which gives uncoupled differential equations with single-decay exponential solutions. This approximation can be applied to our experimental system because the characteristic frequencies of the internal interactions, ω_L and ω_Q , are much

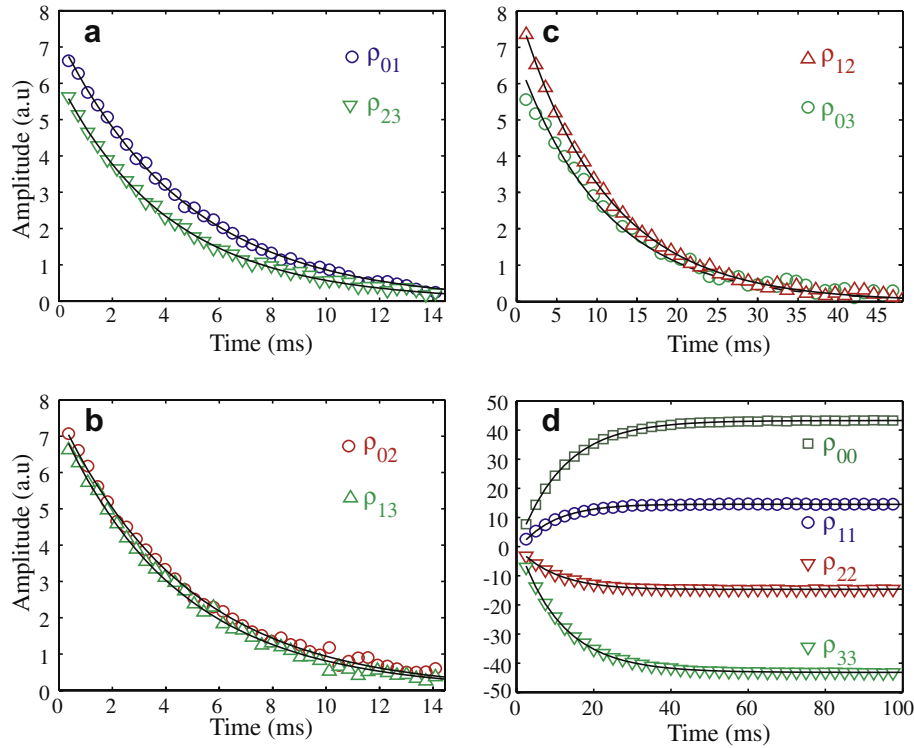


Fig. 5. Experimental data (symbols) and correspondent fittings (solid line) of the density matrix elements for the pseudo-pure state $|\text{sup}\rangle$.

Table 2

Reduced spectral densities obtained from the relaxation of the density matrix diagonal elements of the pseudo-pure states

Parameters	Pseudo-pure states						Average
	$ 00\rangle$	$ 01\rangle$	$ 10\rangle$	$ 11\rangle$	$ \text{cat}\rangle$	$ \text{sup}\rangle$	
$J_1 (\times 10^{-9} \text{ s})$	3.8 ± 0.7	3.1 ± 0.3	3.5 ± 0.7	3.1 ± 0.3	3.2 ± 0.3	3.8 ± 0.4	3.4 ± 0.4
$J_2 (\times 10^{-9} \text{ s})$	3.6 ± 0.3	3.6 ± 0.3	3.7 ± 0.3	3.7 ± 0.3	3.8 ± 0.3	3.6 ± 0.3	3.7 ± 0.3

greater than the relaxation rates. The fact that our SDS system presents this behavior (note that the secular approach was not assumed a priori) indicates that the relaxation is mostly defined by the local quadrupolar coupling, which is actually consistent given the dilution of the ^{23}Na ions in SDS. This conclusion is based on the fact that in a multi-spin system cross-terms would be certainly important for the relaxation [57]. The use of the secular approximation also explains why we have optimized just the diagonal elements of the basis states, disregarding their coherence values. Since, from the secular approximation, the populations relax independently of the coherences, the last ones can assume any arbitrary value.

Therefore, the use of QST made possible the experimental characterization of the relaxation of all density matrix elements in a spin 3/2 quadrupolar system. The proper modelling using the Redfield theory allowed determining the relaxation parameters with good accuracy.

3.2.3. Relaxation model for the SDS nematic liquid crystal

Once the reduced spectral densities were determined, it is important to discuss whether the obtained values are consistent with a specific relaxation model. The relaxation of

the N_C nematic phase of the SDS liquid crystal was earlier characterized using standard relaxation measurements [56,54]. In these references the relaxation was described using the so called two-step models that assume that the motions are composed by a fast component in the extreme narrowing regime and a slow component, so the total reduced spectral densities can be written as [55,56]:

$$J_n = (1 - S^2)J_n^f + S^2J_n^s \quad (30)$$

$$J_n = 2(1 - S^2)\tau_C^f + S^2 \frac{\tau_C^s}{1 + (n\omega\tau_C^s)^2}, \quad (31)$$

where S is the order parameter to account for the system anisotropy. Note that for a N_C phase it can be taken as the same as S_{DN} . J_n^f is the reduced spectral density for the local fast motion, which is assumed to be isotropic because the ionic exchange inside the liquid crystal micelle, and J_n^s is the reduced spectral density for the slow motion ascribed to the motion of the entire micelle and to surfactant diffusion over the curved micellar surface [56]. The first feature to be noticed is that, without assuming any specific model for the relaxation mechanism (we just assumed pure quadrupolar relaxation), we found $J_0 > J_1 \approx J_2$. As stated in reference [52], this behavior is expected when free ions

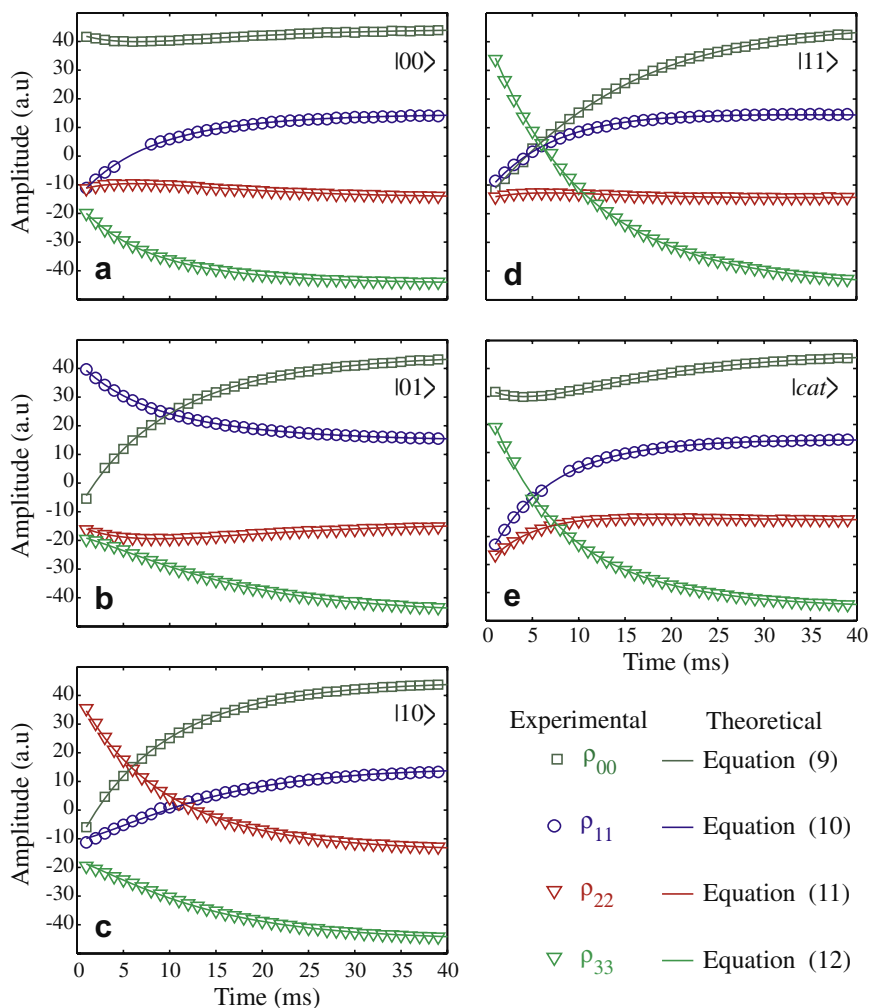


Fig. 6. Experimental data (symbols) and corresponding fittings (solid line) of the diagonal density matrix elements for the pseudo-pure states (a) $|00\rangle$, (b) $|01\rangle$, (c) $|10\rangle$, (d) $|11\rangle$, and (e) $|cat\rangle$.

exchange with a small population of ions bound to macromolecules. Thus, this result shows by itself that the two-step model is appropriated for the SDS system. The evaluation of the correlation times τ_c^s and τ_c^f can be done by noting that:

$$J_0 - J_1 = S_{\text{DN}}^2 \tau_c^s - S_{\text{DN}}^2 \frac{\tau_c^s}{1 + (\omega \tau_c^s)^2}, \quad (32)$$

$$J_0 - J_2 = S_{\text{DN}}^2 \tau_c^s - S_{\text{DN}}^2 \frac{\tau_c^s}{1 + (2\omega \tau_c^s)^2}. \quad (33)$$

Hence, these combinations provide equations that depend only on τ_c^s . Therefore, using the reduced spectral density values shown in Table 1, $S = -0.3$, and Eq. (32) one find $\tau_c^s = (120 \pm 10)$ ns. Replacing τ_c^s in Eq. (30) one obtain $\tau_c^f = (1.9 \pm 0.9)$ ns with $n = 0$. Thus, the individual evaluation of J_0 , J_1 , and J_2 , provided by the method described in this article, can be interpreted as a way of separating the slow and the fast motion contributions to the relaxation. It is worth mention that the main aim here was to show that the obtained values for the reduced spectral densities were consistent with a previous model

adopted for the ^{23}Na relaxation in SDS. A complete relaxation study must certainly involve measurements as a function of temperature and orientation, such as done in reference [54]. However, all these experiments can be done using QST, with the advantage of a probably less ambiguous estimation of the reduced spectral densities. The method can be extended to other spin values and also to take into account the dipolar contribution to the relaxation based on references [52,57].

4. Coherence loss of a two-qubit system

In the previous sections we described how to determine the reduced spectral densities by following the system evolution of the quantum states until the thermal equilibrium is reached. In this section we continue to explore that, but now from the Quantum Computing point of view, in a sense that a quadrupolar nuclei ($I = 3/2$), under a magnetic field and electric field gradient, may emulate a two-qubit system [35,45–51]. Since we obtained the full density matrix at several time intervals during the relaxation pro-

cess, it is possible to study the quantum state of each qubit separately using the partial trace operation [2]. By doing so, the density matrices of the individual qubits become,

$$\rho_A(t) = \begin{bmatrix} \rho_{00}(t) + \rho_{11}(t) & \rho_{02}(t) + \rho_{13}(t) \\ \rho_{02}^\dagger(t) + \rho_{13}^\dagger(t) & \rho_{22}(t) + \rho_{33}(t) \end{bmatrix}, \quad (34)$$

$$\rho_B(t) = \begin{bmatrix} \rho_{00}(t) + \rho_{22}(t) & \rho_{01}(t) + \rho_{23}(t) \\ \rho_{01}^\dagger(t) + \rho_{23}^\dagger(t) & \rho_{11}(t) + \rho_{33}(t) \end{bmatrix}, \quad (35)$$

As it may be seen, while the double quantum coherences of the original density matrix determine the off-diagonal elements of the first qubit density matrix (labeled as A , $\rho_A(t)$), the original single quantum coherences define the second qubit density matrix off-diagonal elements (labeled as B , $\rho_B(t)$). Note also that the single quantum $\rho_{12}(t)$ and the triple quantum $\rho_{03}(t)$ coherences do not contribute to the qubits density matrix. This shows, as expected, that entanglement effects cannot be detected only by the observation of the individual qubits. Rewriting Eqs. (34) and (35) in terms of Eqs. (8)–(17) we find:

$$\rho_A(t) = \begin{bmatrix} \rho_{00}^{\text{eq}} + \rho_{11}^{\text{eq}} + \frac{1}{2}(R_2^0 e^{-2CJ_2 t}) & (\rho_{02}^0 + \rho_{13}^0) e^{-C(J_0+J_2)t} \\ (\rho_{02}^{0\dagger} + \rho_{13}^{0\dagger}) e^{-C(J_0+J_2)t} & \rho_{22}^{\text{eq}} + \rho_{33}^{\text{eq}} - \frac{1}{2}(R_2^0 e^{-2CJ_2 t}) \end{bmatrix}, \quad (36)$$

$$\rho_B(t) = \begin{bmatrix} \rho_{00}^{\text{eq}} + \rho_{22}^{\text{eq}} + \frac{1}{2}(R_3^0 e^{-2CJ_1 t}) & (\rho_{01}^0 + \rho_{23}^0) e^{-C(J_0+J_1)t} \\ (\rho_{01}^{0\dagger} + \rho_{23}^{0\dagger}) e^{-C(J_0+J_1)t} & \rho_{11}^{\text{eq}} + \rho_{33}^{\text{eq}} - \frac{1}{2}(R_3^0 e^{-2CJ_1 t}) \end{bmatrix}. \quad (37)$$

Therefore, all elements of the density matrix of both qubits show single-exponential decays. The diagonal elements of qubits A and B depend on the J_2 and J_1 reduced spectral densities, respectively. Furthermore, the off-diagonal elements decay with different rates for each qubit: $C(J_0 + J_2)$ and $C(J_0 + J_1)$ for qubits A and B , respectively.

The magnetization corresponding to the k component of the angular momentum operator ($I = 1/2$) is given by [40]:

$$M_k^{A,B}(t) = \langle \mathbf{I}_k \rangle = \sum_i \{ \rho_{A,B}(t) \mathbf{I}_k \}_{ii}. \quad (38)$$

Then, considering the quadrupolar system as a two-qubit system, the individual magnetization for each qubit can be written as:

$$M_x^A(t) = \mathbf{Re}(\rho_{02}^0 + \rho_{13}^0) e^{-C(J_0+J_2)t}, \quad (39)$$

$$M_y^A(t) = \mathbf{Im}(\rho_{02}^0 + \rho_{13}^0) e^{-C(J_0+J_2)t}, \quad (40)$$

$$M_z^A(t) = 2p + R_2^0 e^{-2CJ_2 t}. \quad (41)$$

$$M_x^B(t) = \mathbf{Re}(\rho_{01}^0 + \rho_{23}^0) e^{-C(J_0+J_1)t}, \quad (42)$$

$$M_y^B(t) = \mathbf{Im}(\rho_{01}^0 + \rho_{23}^0) e^{-C(J_0+J_1)t}, \quad (43)$$

$$M_z^B(t) = p + R_3^0 e^{-2CJ_1 t}. \quad (44)$$

Thus, it is possible to draw two main conclusions:

- The decoherence rates for the two qubits may be different, being $C(J_0 + J_2)$ for qubit A and $C(J_0 + J_1)$ for qubit B . However, in our specific case, where $[C(J_0 + J_2)] = [C(J_0 + J_1)] = (210 \pm 10)s^{-1}$, this difference could not be detected.
- The relaxation rates for the diagonal elements are also different upon distinct qubits. While it is $(2CJ_2)^{-1}$ for qubit A , $((2CJ_2)^{-1} = (90 \pm 10)s^{-1}$ in our system), for qubit B it is given by $(2CJ_1)^{-1}$, $(2CJ_2)^{-1} = (80 \pm 10)s^{-1}$ in our system).

In a system of two coupled spin 1/2 the qubits can be directly identified as individual nuclear spins. Thus, the magnetization associated with each qubit can also be assigned as the magnetization of the individual spin. The relaxation of two coupled spins 1/2 (named spin σ and η) was early described in the seminal article of Solomon [24]. In this article he showed that the decay of the transverse magnetization of both spins are exponential with decoherence rates given by $2(u_1 + u_2)$ for spin σ and $2(u_1' + u_2')$ for spin η , see Table 3. u_1 , u_2 , and u_1' are related with the proper reduced spectral densities according to reference [24]. This behavior is perfectly emulated by the quadrupolar spin 3/2 system, where the decay of the transverse magnetization of the qubits is also exponential and given by $C(J_0 + J_2)$ and $C(J_0 + J_1)$, respectively. However, as shown in Table 3, for the spin 1/2 system the recovery of the longitudinal magnetization is biexponential, which is not the same case for the quadrupolar system, where purely exponential decay is observed for both qubits. Therefore, despite the quadrupolar spin 3/2 can emulate the decoherence of the spin 1/2 system, it cannot emulate completely the relaxation of the system (see Table 4).

5. Conclusions

In this article we have analyzed the relaxation of a spin 3/2 quadrupolar system using QST. From the experimentally determined evolution of the density matrices of sev-

Table 3

Theoretical expressions for the density matrices elements of the first qubit considering a spin 1/2 system (σ) and a quadrupolar spin 3/2 system (A)

	Spin σ	Qubit A
Transverse relaxation rate	$2(u_1 + u_2)$	$C(J_0 + J_2)$
Real part of the transverse component	$(\sigma_{12}^0 + \sigma_{12}^{0\dagger})$	$(\rho_{02}^0 + \rho_{13}^0 + \rho_{02}^{0\dagger} + \rho_{13}^{0\dagger})$
Imaginary part of the transverse component	$(\sigma_{12}^0 - \sigma_{12}^{0\dagger})$	$(\rho_{02}^0 + \rho_{13}^0 - \rho_{02}^{0\dagger} - \rho_{13}^{0\dagger})$
Longitudinal relaxation rate	λ_1, λ_2	$2CJ_2$
Longitudinal component	$A_\sigma e^{\lambda_1(t-t_0)} + B_\sigma e^{\lambda_2(t-t_0)}$	$R_2^0 e^{-2CJ_2(t-t_0)}$
Equilibrium state value	$(\sigma_{11}^{\text{eq}} - \sigma_{22}^{\text{eq}})$	$(\rho_{00}^{\text{eq}} + \rho_{11}^{\text{eq}} - \rho_{22}^{\text{eq}} - \rho_{33}^{\text{eq}})$

Table 4

Theoretical expressions for the density matrices elements of the second qubit considering a couple spin 1/2 system (η), a quadrupolar spin 3/2 system (B)

	Spin η	Qubit B
Transverse relaxation rate	$2(u'_1 + u_2)$	$C(J_0 + J_1)$
Real part of the transverse component	$(\eta_{12}^0 + \eta_{12}^{0i})$	$(\rho_{01}^0 + \rho_{23}^0 + \rho_{01}^{0i} + \rho_{23}^{0i})$
Imaginary part of the transverse component	$(\eta_{12}^0 - \eta_{12}^{0i})$	$(\rho_{01}^0 + \rho_{23}^0 - \rho_{01}^{0i} - \rho_{23}^{0i})$
Longitudinal relaxation rate	λ_1, λ_2	$2CJ_1$
Longitudinal component	$A_\eta e^{\lambda_1(t-t_0)} + B_\eta e^{\lambda_2(t-t_0)}$	$R_3^0 e^{-2CJ_1(t-t_0)}$
Equilibrium state value	$(\eta_{11}^{eq} - \eta_{22}^{eq})$	$(\rho_{00}^{eq} + \rho_{22}^{eq} - \rho_{11}^{eq} - \rho_{33}^{eq})$

eral initial states we obtained the reduced spectral densities J_k 's using the Redfield formalism and assuming pure quadrupolar relaxation. The obtained reduced spectral densities were analyzed considering a two-step relaxation model that assumes fast and slow relaxation components, whose the corresponding relaxation times were determined. As usually found in liquid crystals, this two-step model is consistent with the presence of free motion of the Na ions inside de liquid crystal micelle and the slow component ascribed to the motion of the entire micelle and to surfactant diffusion over the curved micellar surface. Furthermore, considering the Quantum Information point of view that a spin 3/2 system is equivalent to a two-qubit system, we characterized the relaxation of the individual qubits by applying the partial trace operation on the original density matrices. The theoretical equations showed that a qubit can loose coherence faster than the other, in the same way as experimentally observed by Tseng et al. [10] for spin half systems. However, for our experimental system, we found $J_1 \approx J_2$, which implies equal relaxation times for the magnetization of both qubits. We also explored the possibility of emulating the relaxation of other quantum systems using the spin 3/2 NMR system. It was found that only the decoherence of the coupled spin 1/2 system can be properly reproduced.

Acknowledgments

The authors acknowledge the financial support of the Brazilian Science Foundations CAPES, CNPq, and FAPESP. We specially acknowledge the support of the Conselho Nacional de Desenvolvimento Científico e Tecnológico (CNPq) in the framework of the network project *Millennium Institute for Quantum Information*.

References

- [1] I.S. Oliveira, T.J. Bonagamba, R.S. Sarthour, J.C.C. Freitas, E.R. deAzevedo, NMR Quantum Information Processing, Elsevier, Amsterdam, 2007.
- [2] M.A. Nielsen, I.L. Chuang, Quantum computation and quantum information, Cambridge University Press, 2000.

- [3] N. Linden, H. Barjat, R. Freeman, An implementation of the Deutsch-Jozsa algorithm on a three-qubit NMR quantum computer, Chem. Phys. Lett. 296 (1998) 61–67.
- [4] J.A. Jones, M. Mosca, Implementation of a quantum algorithm on a nuclear magnetic resonance quantum computer, J. Chem. Phys. 109 (1998) 1648–1653.
- [5] I.L. Chuang, L.M.K. Vandersypen, X. Zhou, D.W. Leung, S. Lloyd, Experimental realization of a quantum algorithm, Nature 393 (1998) 143–146.
- [6] Jonathan A. Jones, Michele Mosca, Rasmus H. Hansen, Implementation of a quantum search algorithm on a quantum computer, Nature 393 (1998) 344–346.
- [7] L.M.K. Vandersypen, M. Steffen, G. Breyta, C.S. Yannoni, M.H. Sherwood, I.L. Chuang, Experimental realization of Shor's quantum factoring algorithm using nuclear magnetic resonance, Nature 414 (2001) 883–887.
- [8] M.A. Nielsen, E. Knill, R. Laflamme, Complete quantum teleportation using nuclear magnetic resonance, Nature 396 (1998) 52–55.
- [9] S. Somaroo, C.H. Tseng, T.F. Havel, R. Laflamme, D.G. Cory, Quantum simulations on a quantum computer, Phys. Rev. Lett. 85 (1999) 5381–5384.
- [10] C.H. Tseng, S. Somaroo, Y. Sharf, E. Knill, R. Laflamme, T.F. Havel, D.G. Cory, Quantum simulation with natural decoherence, Phys. Rev. A 62 (2000) 032309.
- [11] A.K. Khitrin, B.M. Fung, NMR simulation of an eight-state quantum system, Phys. Rev. A 64 (2001) 032306.
- [12] E. Knill, R. Laflamme, R. Martinez, C.H. Tseng, An algorithmic benchmark for quantum information processing, Nature 404 (2000) 368–370.
- [13] M. Lovric, H.G. Krojanski, D. Suter, Decoherence in large quantum registers under variable interaction with the environment, Phys. Rev. A 75 (2007) 042305.
- [14] H.G. Krojanski, D. Suter, Decoherence in large NMR quantum registers, Phys. Rev. A 74 (2006) 062319.
- [15] H.G. Krojanski, D. Suter, Scaling of decoherence in wide NMR quantum registers, Phys. Rev. Lett. 93 (2004) 090501.
- [16] F.M. Cucchiatti, J.P. Paz, W.H. Zurek, Decoherence from spin environments, Phys. Rev. A 72 (2005) 052113.
- [17] F.M. Cucchiatti, S. Fernandez-Vidal, J.P. Paz, Universal decoherence induced by an environmental quantum phase transition, Phys. Rev. A 75 (2007) 032337.
- [18] Gonzalo A. Alvarez, Ernesto P. Danieli, Patricia R. Levstein, Horacio M. Pastawski, Decoherence under many-body system-environment interactions: a stroboscopic representation based on a fictitiously homogenized interaction rate, Phys. Rev. A 75 (2007) 062116.
- [19] Davide Rossini, Tommaso Calarco, Vittorio Giovannetti, Simone Montangero, Rosario Fazio, Decoherence induced by interacting quantum spin baths, Phys. Rev. A 75 (2007) 032333.
- [20] E. Fraval, M.J. Sellars, J.J. Longdell, Dynamic decoherence control of a solid-state nuclear-quadrupole qubit, Phys. Rev. Lett. 95 (2005) 030506.
- [21] Jingfu Zhang, Xinhua Peng, Nageswaran Rajendran, Dieter Suter, Effect of system level structure and spectral distribution of the environment on the decoherence rate, Phys. Rev. A 75 (2007) 042314.
- [22] N. Bloembergen, E.M. Purcell, R.V. Pound, Relaxation effects in nuclear magnetic resonance absorption, Phys. Rev. 73 (1948) 679–712.
- [23] R. Kubo, K. Tomita, A general theory of magnetic resonance absorption, J. Phys. Soc. Jpn. 9 (1954) 888–919.
- [24] I. Solomon, Relaxation processes in a system of two spins, Phys. Rev. 99 (1955) 559–565.
- [25] A.G. Redfield, On the theory of relaxation processes, IBM J. Res. Dev. 1 (1957) 19–31.
- [26] J.A. Pople, The effect of quadrupole relaxation on nuclear magnetic resonance multiplets, Mol. Phys. 1 (1958) 168–174.
- [27] Paul S. Hubbard, Nonexponential nuclear magnetic relaxation by quadrupole interactions, J. Chem. Phys. 53 (1970) 985–987.

- [28] J. McConnell, Nuclear magnetic relaxation by quadrupole interactions in non-spherical molecules, *Physica A* 117 (1983) 251–264.
- [29] A. Suter, M. Mali, J. Roos, D. Brinkmann, Mixed magnetic and quadrupolar relaxation in the presence of a dominant static Zeeman hamiltonian, *J. Phys. Condens. Matter* 10 (1998) 5977–5994.
- [30] I. Furó, B. Halle, T.C. Wong, Spin relaxation of $I > 1$ nuclei in anisotropic systems. I. Two dimensional quadrupolar echo Fourier spectroscopy, *J. Chem. Phys.* 89 (1988) 5382–5397.
- [31] I. Furó, B. Halle, Multiple quantum NMR spectroscopy on $I > 1$ nuclei in anisotropic systems, *Mol. Phys.* 76 (1992) 1169–1197.
- [32] D.E. Woessner, NMR relaxation of spin- $\frac{3}{2}$ nuclei: Effects of structure, order, and dynamics in aqueous heterogeneous systems, *Concepts Magn. Reson.* 13 (2001) 294–325.
- [33] Johan R.C. Van der Maarel, Thermal relaxation and coherence dynamics of spin $\frac{3}{2}$. I. Static and fluctuating quadrupolar interactions in the multipole basis, *Concepts Magn. Reson. Part A* 19A (2003) 97–116.
- [34] Johan R.C. Van der Maarel, Relaxation of spin quantum number $S = 3/2$ under multiple-pulse quadrupolar echoes, *J. Chem. Phys.* 94 (1991) 4765–4775.
- [35] R.S. Sarthour, E.R. deAzevedo, F.A. Bonk, E.L.G. Vidoto, T.J. Bonagamba, A.P. Guimarães, J.C.C. Freitas, I.S. Oliveira, Relaxation of coherent states in a two-qubit NMR quadrupole system, *Phys. Rev. A* 68 (2003) 022311.
- [36] Martin Laforest, Damien Simon, Jean-Christian Boileau, Jonathan Baugh, Michael J. Ditty, Raymond Laflamme, Using error correction to determine the noise model, *Phys. Rev. A* 75 (2007) 012331.
- [37] A. Ghosh, A. Kumar, Relaxation of pseudo pure states: the role of cross-correlations, *J. Magn. Reson.* 173 (2005) 125–133.
- [38] E.M. Fortunato, M.A. Pravia, N. Boulant, G. Teklemariam, T.F. Havel, D.G. Cory, Design of strongly modulating pulses to implement precise effective hamiltonians for quantum information processing, *J. Chem. Phys.* 116 (2002) 7599–7606.
- [39] H. Kampermann, W.S. Veeman, Characterization of quantum algorithms by quantum process tomography using quadrupolar spins in solid-state nuclear magnetic resonance, *J. Chem. Phys.* 122 (2005) 214108.
- [40] A. Abragam, *Principles of Nuclear Magnetism*, Oxford Science Publications, reprinted, 1994.
- [41] A.D. McLachlan, Line widths of electron resonance spectra in solution, *Proc. R. Soc. Lond. Ser. A* 280 (1964) 271–288.
- [42] J. McConnell, *The Theory of Nuclear Magnetic Relaxation in Liquids*, Cambridge University Press, 1987.
- [43] G. Jaccard, S. Wimperis, G. Bodenhausen, Multiple-quantum NMR spectroscopy of $S = 3/2$ spins in isotropic phase: a new probe for multiexponential relaxation, *J. Chem. Phys.* 85 (1986) 6282–6293.
- [44] J. Teles, E.R. deAzevedo, R. Auccaise, R.S. Sarthour, Ivan S. Oliveira, T.J. Bonagamba, Quantum state tomography for quadrupolar nuclei using global rotations of the spin system, *J. Chem. Phys.* 126 (2007) 154506.
- [45] A.R. Kessel, V.L. Ermakov, Multiqubit spin, *JETP Lett.* 70 (1999) 61–65.
- [46] N. Sinha, T.S. Mahesh, K.V. Ramanathan, A. Kumar, Toward quantum information processing by nuclear magnetic resonance: pseudopure states and logical operations using selective pulses on an oriented spin $3/2$ nucleus, *J. Chem. Phys.* 114 (2001) 4415–4420.
- [47] A.K. Khitrin, B.M. Fung, Nuclear magnetic resonance quantum logic gates using quadrupolar nuclei, *J. Chem. Phys.* 112 (2000) 6963–6965.
- [48] R. Das, A. Kumar, Use of quadrupolar nuclei for quantum-information processing by nuclear magnetic resonance: implementation of a quantum algorithm, *Phys. Rev. A* 68 (2003) 032304.
- [49] H. Kampermann, W.S. Veeman, Quantum computing using quadrupolar spins in solid state NMR, *Quantum Inf. Process.* 1 (2002) 327–344.
- [50] A. Bonk, E.R. deAzevedo, R.S. Sarthour, J.D. Bulnes, J.C.C. Freitas, A.P. Guimarães, I.S. Oliveira, T.J. Bonagamba, Quantum logical operations for spin $3/2$ quadrupolar nuclei monitored by quantum state tomography, *J. Magn. Reson.* 175 (2005) 226–234.
- [51] A. Bonk, R.S. Sarthour, E.R. deAzevedo, J.D. Bulnes, G.L. Mantovani, J.C.C. Freitas, T.J. Bonagamba, A.P. Guimarães, I.S. Oliveira, Quantum state tomography for quadrupole nuclei and its applications on a two-qubit system, *Phys. Rev. A* 69 (2004) 042322.
- [52] U. Eliav, G. Navon, Measurement of dipolar interaction of quadrupolar nuclei in solution using multiple-quantum nmr spectroscopy, *J. Magn. Reson. Ser. A* 123 (1996) 32–48.
- [53] J.F. Hon, P.J. Bray, Nuclear quadrupole coupling constant of ${}^7\text{Li}$ in lithium compounds, *Phys. Rev.* 110 (1958) 624–629.
- [54] P. Quist, B. Halle, I. Furó, Micelle size and order in lyotropic nematic phases from nuclear spin relaxation, *J. Chem. Phys.* 96 (1952) 3875–3891.
- [55] B. Halle, H. Wennerstrom, Study of lyotropic nematic phases from nuclear spin relaxation, *J. Chem. Phys.* 75 (1981) 1928–1937.
- [56] L. Tsoref, U. Eliav, G. Navon, Nuclear magnetic resonance relaxation in micelles, *J. Chem. Soc., Faraday Trans.* 84 (1988) 4475–4486.
- [57] O. Soderman, G. Carlstrom, U. Olsson, T.C. Wong, Multiple quantum filtered nuclear magnetic resonance spectroscopy of spin $7/2$ nuclei in solution, *J. Chem. Soc., Faraday Trans.* 1044 (1996) 3463–3471.